Journal of Alloys and Compounds 638 (2015) 214–220

Contents lists available at ScienceDirect

Journal of Alloys and Compounds

journal homepage: www.elsevier.com/locate/jalcom

Preparation and characterization of $Fe_3O_4/SiO_2/Bi_2MoO_6$ composite as magnetically separable photocatalyst

Xuemei Hou [a,1], Yanlong Tian [b,1], Xiang Zhang [b], Shuliang Dou [b], Lei Pan [b], Wenjia Wang [b], Yao Li [b], Jiupeng Zhao [a,*]

[a] School of Chemical Engineering and Technology, Harbin Institute of Technology, No. 92, Xidazhi Street, Nangang District, Harbin, China
[b] Center for Composite Materials, Harbin Institute of Technology, Harbin, China

ARTICLE INFO

Article history:
Received 22 January 2015
Received in revised form 2 March 2015
Accepted 5 March 2015
Available online 11 March 2015

Keywords:
Magnetic
Bi_2MoO_6
Composite
Photocatalyst

ABSTRACT

In this paper, $Fe_3O_4/SiO_2/Bi_2MoO_6$ microspheres were prepared by a facile hydrothermal method. The scanning electron microscope (SEM) results revealed that flower-like three dimensional (3D) Bi_2MoO_6 microspheres were decorated with Fe_3O_4/SiO_2 magnetic nanoparticles. The UV–vis diffuse reflection spectra showed extended absorption within the visible light range compared with pure Bi_2MoO_6. We evaluated the photocatalytic activities of $Fe_3O_4/SiO_2/Bi_2MoO_6$ microspheres on the degradation of Rhodamine B (RhB) under visible light irradiation and found that the obtained composite exhibited higher photocatalytic activity than pure Bi_2MoO_6 and P25. Moreover, the $Fe_3O_4/SiO_2/Bi_2MoO_6$ composite also displayed excellent stability and their photocatalytic activity decreased slightly after reusing 5 cycles. Meanwhile, the composite could be easily separated by applying an external magnetic field. The trapping experiment results suggest that superoxide radical species O_2^- and hydroxyl radicals ·OH play a major role in $Fe_3O_4/SiO_2/Bi_2MoO_6$ system under visible light irradiation. The combination of flower-like three dimensional (3D) Bi_2MoO_6 microspheres and Fe_3O_4/SiO_2 magnetic nanospheres provides a useful strategy for designing multifunctional nanostructure materials with enhanced photocatalytic activities in the potential applications of water purification.

1. Introduction

Many concepts to harvest and store sustainable energy sources (sunlight, wind, water) directly or from secondary process are under development to reduce our dependence on fossil energy sources. Among all kinds of green earth and renewable energy projects underway, semiconductor photocatalysis has received wide interest because it provides an easy way to directly utilize the energy of either natural sunlight or artificial indoor illumination [1–4]. Along this line, abundant photocatalytic materials (such as metal oxides, sulfides, and oxynitrides) have been developed in the degradation of organic contaminants and splitting of water [5–7]. Nevertheless, there is still a problem related to difficult recovery of photocatalyst nanoparticles from the mixed system. Therefore, it is a key link to seek simple methods of recovering photocatalyst nanoparticles for large-scale application of photocatalytic processes.

The introduction of magnetic materials is an effective method to effortlessly separate and recover photocatalyst nanoparticles by applying an external magnetic field [8,9]. These magnetically separable photocatalysts have displayed novel optical, magnetic, or catalytic properties in comparison with their individual single-component materials [10]. Especially iron oxide is a most frequently used magnetic component for constructing magnetically separable photocatalysts due to its superparamagnetism that superparamagnetic materials are not subject to strong magnetic interactions in dispersion. As a consequence, several iron oxide based magnetically separable photocatalysts have been designed, such as Fe_3O_4–TiO_2 [11], Fe_3O_4–BiOCl [12], Fe_3O_4–Ag_3PO_4 [13], Fe_3O_4/SiO_2–TiO_2 [14], Fe_3O_4–Bi_2O_3 [15], Bi_2WO_6/carbon/Fe_3O_4 [16], Fe_3O_4–BiOI [17] and Fe_3O_4–SiO_2–Bi_2WO_6 [18].

Bismuth molybdate (Bi_2MoO_6) as an important Ternary bismuth oxide compound has received considerable attention because of its intrinsic properties, such as dielectric nature, catalytic behavior and luminescence [19–21]. Ternary bismuth oxide compounds, Bi–M–O (M = Mo, W, V, Nb or Ta) possess a typical Aurivillius layered structure consisting of perovskite octahedral $(MO_4)^{2-}$ sheets sandwiched between $(Bi_2O_2)^{2+}$ layers [22–24]. Such a layered

* Corresponding author. Tel./fax: +86 451 86403767.
E-mail address: jiupengzhao@126.com (J. Zhao).
[1] These authors contributed equally to this study.

http://dx.doi.org/10.1016/j.jallcom.2015.03.039
0925-8388/

structure is conducive to charge transfer, and thereby could suppress the recombination of photogenerated carriers. What is more, Bi_2MoO_6 dispalys a typical band gap of about 2.60 eV [25]. These excellent structural and spectral properties imply that Bi_2MoO_6 should be a promising photocatalyst [26–29]. Not surprisingly, recently studies confirmed that Bi_2MoO_6 has excellent visible-light-driven photocatalytic activities for water splitting and the degradation of organic pollutants [30,31]. Despite these advantages of Bi_2MoO_6, it is still challenging to simply recover nanopowders from the solution.

Herein, magnetically separable $Fe_3O_4/SiO_2/Bi_2MoO_6$ composite was prepared via a facile hydrothermal method. In the obtained $Fe_3O_4/SiO_2/Bi_2MoO_6$ composite, flower-like three dimensional (3D) Bi_2MoO_6 microspheres were decorated with Fe_3O_4/SiO_2 magnetic nanoparticles, and thus formed a hierarchical structure. The visible light photocatalytic tests show that the present $Fe_3O_4/SiO_2/Bi_2MoO_6$ composite possess excellent photocatalytic activity for degrading RhB. After the photocatalytic reaction has been completed, the composite can be easily collected for reuse by applying an external magnetic field.

2. Materials and methods

All chemicals were analytical grade and used without further purification. Deionized water (18 MΩ cm^{-1}) was used for all experiments.

2.1. Preparation of monodisperse Fe_3O_4 nanoparticles

The magnetic Fe_3O_4 nanoparticle was synthesized according to a previous report with a little modification [32]. In a typical process, 1.3 g of $FeCl_3{\cdot}6H_2O$ was dissolved in 40 mL ethylene glycol to form a clear solution. Then 0.4 g of trisodium citrate and 2.4 g of sodium acetate were added under vigorous stirring. After vigorously stirring for 30 min, the resulting homogeneous dispersion was transferred into a Teflon-lined stainless-steel autoclave with a capacity of 80 mL, sealed, heated at 200 °C and maintained for 10 h. The as-prepared products were collected with a magnet and washed with ethanol and deionized water for several times, then dried at 60 °C under vacuum for further use.

2.2. Preparation of Fe_3O_4/SiO_2 nanoparticles

The synthesis of Fe_3O_4/SiO_2 nanoparticle was carried out by a modified sol–gel method [33]. Typically, 0.1 g as-prepared Fe_3O_4 nanoparticles were treated with 0.1 M HCl aqueous solution (50 mL) by ultrasonication. After the treatment for 10 min, the magnetite particles were separated, washed with water, and then homogeneously dispersed in the mixture of 40 mL ethanol and 10 mL deionized water by ultrasonication for about 10 min. Subsequently, 1 mL ammonia solution was added in the above solution under continuous mechanical stirring, and followed 0.1 mL TEOS was added dropwise. Finally, the reaction was allowed to proceed at room temperature for 6 h. The resulting products were washed with ethanol and dried at 60 °C under vacuum.

2.3. Preparation of $Fe_3O_4/SiO_2/Bi_2MoO_6$ composite

A facile hydrothermal method was used for the immobilization of Fe_3O_4/SiO_2 nanoparticles onto the surface of Bi_2MoO_6 to obtain $Fe_3O_4/SiO_2/Bi_2MoO_6$ composite. Briefly, 0.97 g (2 mmol) of $Bi(NO_3)_3{\cdot}5H_2O$ and 0.03 g Fe_3O_4/SiO_2 nanoparticles were added in 5 mL of HNO_3 (2 M) solution at room temperature, and then the mixture was sonicated for 30 min. After aging for 2 h, 30 mL of $Na_2MoO_4{\cdot}2H_2O$ (1 mmol) solution was added. The mixture was sonicated at room temperature for another 30 min before being transferred to a stainless steel autoclave with a Teflon liner of 80 mL capacity and maintained at 160 °C for 12 h. After the autoclave had been cooled to room temperature, the products were harvested using a magnet, and subject to several cycles of magnetic separation/washing/redispersion before being dried at room temperature. Pure Bi_2MoO_6 microspheres prepared without Fe_3O_4/SiO_2 were used for comparison.

2.4. Characterization

Powder X-ray diffraction (XRD) patterns of the prepared products were carried out on a Dmax-rA powder diffractometer, Cu Kα as a radiation source with an operating voltage of 40 kV and an operating current of 40 mA. The morphologies and sizes of the as-prepared samples were characterized by scanning electron microscopy (SEM, FEI Helios Nanolab 600i) equipped with an energy dispersive X-ray analyzer (EDX) and Transmission Electron Microscopy (TEM, H-7650, Hitachi) with an accelerating voltage of 100 kV. Fourier transform infrared (FT-IR) spectra were collected in the range of 4000–400 cm^{-1} on a FT-IR spectrum (AVATAR 360, Nicolet) using the KBr pellet method at room temperature. Magnetic properties at room temperature were measured by a vibrating sample magnetometer (VSM, Lake Shore7407) in a maximum field of 15kOe. UV–Vis absorption spectrum was investigated by UV–Vis spectrometer (Perkin Elmer, lambda 950) with the wavelength ranging from 200 to 800 nm.

2.5. Photocatalytic tests

Photocatalytic activities of the as-prepared samples were evaluated by degradation of Rhodamine B (RhB) under visible light irradiation. A 300 W xenon lamp with a cut-off filter was used as the visible light source. Briefly, 100 mg of photocatalyst was suspended in 100 mL of RhB solution (10 mg L^{-1}) with constant stirring. Before illumination, the suspension was stirred in the dark for 1 h to establish adsorption–desorption equilibrium. The temperature of the system was controlled at room temperature by circulating cooing water. At the given time intervals, 3 mL of mixture was collected and separated by a magnet. The concentration of the resulting supernatant was monitored by checking the absorbance at 553 nm using Lambda 950 spectrophotometer. In the recycle reaction, the catalyst was separated by an external magnetic field, the recycled catalyst was washed with ethanol and deionized water several times before being re-dispersed in the dye solution(100 mL, 10 mg L^{-1})for the next cycling.

3. Results and discussions

3.1. Characterization of $Fe_3O_4/SiO_2/Bi_2MoO_6$ composite

The crystal structure of Fe_3O_4, Fe_3O_4/SiO_2 and $Fe_3O_4/SiO_2/Bi_2MoO_6$ composite were characterized by XRD, as shown in Fig. 1. The pure Fe_3O_4 nanoparticles (Fig. 1a) exhibit feature diffraction peaks at about 30.1°, 35.4°, 43.1°, 53.4°, 57.0° and 62.5° that match well with the (220), (311), (400), (422), (511) and (440) crystal planes of the face-centered cubic (fcc) Fe_3O_4 phase ($a = b = c = 8.397$ Å) as identified using the standard data JCPDS No. 19-0629 [34,35]. No impurity phase is emerged, indicating high purity of Fe_3O_4 nanoparticles. After coating with a SiO_2 layer, in Fig. 1b no new diffraction peaks are observed owing to amorphous phase of the prepared SiO_2. As for $Fe_3O_4/SiO_2/Bi_2MoO_6$ composite, all of the diffraction peaks can be readily indexed to the orthorhombic Bi_2MoO_6 ($a = 5.500$ Å, $b = 16.240$ Å, $c = 5.490$ Å, JCPDS No. 76-2388) [36], with respect to the invisible diffractions of Fe_3O_4 in the composite, this is because the content of Fe_3O_4/SiO_2 is too low.

Fig. 2a–c displays the SEM images of various synthetic stages of $Fe_3O_4/SiO_2/Bi_2MoO_6$ composite. The pristine Fe_3O_4 nanoparticles possess a mean diameter of about 300 nm and near-spherical morphology. Compared with the Fe_3O_4 nanoparticles, although the overall morphology of the obtained Fe_3O_4/SiO_2 nanoparticles (Fig. 2b) is no significant variation, these nanoparticles exhibit more relatively smooth surface. After introducing Bi_2MoO_6, Fe_3O_4/SiO_2 nanoparticles immobilized on flower-like three dimensional (3D) Bi_2MoO_6 microspheres with sizes of ~3 μm, thus the hierarchical structure has been formed. In fact, the flower-like 3D structure of Bi_2MoO_6 are constructed by numerous two dimensional (2D) interlaced nanosheets. Fig. 2d is the EDX elemental microanalysis of $Fe_3O_4/SiO_2/Bi_2MoO_6$ composite, clearly suggesting that Fe, Si, Bi, Mo and O are present in the composite.

The microstructure of Fe_3O_4/SiO_2 nanoparticles and $Fe_3O_4/SiO_2/Bi_2MoO_6$ composite were observed by using TEM technique. In Fig. 3a, the Fe_3O_4 nanoparticles are completely encapsulated into SiO_2 layer with thickness of ~20 nm. The light area with circle shape is silica shell, and the dark area with sphere shape is Fe_3O_4 core, clearly suggesting that the Fe_3O_4/SiO_2 nanoparticles possess a core–shell structure. However, such core–shell structures (small black spheres in Fig. 3b) become invisible due to the large size difference between Bi_2MoO_6 microspheres and $Fe_3O_4@SiO_2$ nanoparticles. Therefore, the small black spheres should be Fe_3O_4/SiO_2 nanoparticles and the large black spheres are Bi_2MoO_6

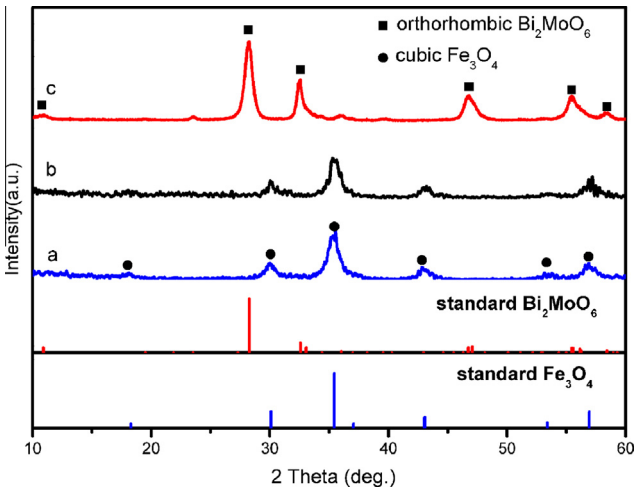

Fig. 1. XRD pattern of (a) Fe_3O_4, (b) Fe_3O_4/SiO_2 and (c) $Fe_3O_4/SiO_2/Bi_2MoO_6$ composite.

microspheres as shown in Fig. 3b. As a result, Bi_2MoO_6 microspheres have magnetism originating from Fe_3O_4 nanoparticles, and become a magnetically separable photocatalyst.

To further confirm the composition, the fourier transform infrared (FT-IR) spectroscopy of Fe_3O_4, Fe_3O_4/SiO_2 and $Fe_3O_4/SiO_2/Bi_2MoO_6$ composite were also investigated. Across the three samples, the wide peak at about 1600 and 3400 cm^{-1} can be ascribed to stretching and bending vibrations of the adsorbed water. In Fig. 4a, the bands at 1611 and 1396 cm^{-1} are associated with carboxylate group. Typical bands assigned to the Fe–O stretching are visible at around 580 cm^{-1}. The new absorption peaks for the Fe_3O_4/SiO_2 nanospheres (Fig. 4b) at 473, 796, 950 and 1086 cm^{-1} are assigned to symmetric and asymmetric stretching vibration of framework and Si–O–Si vibration, suggesting that the Fe_3O_4 was well encapsulated by SiO_2 layer. As for $Fe_3O_4/SiO_2/Bi_2MoO_6$ composite (Fig. 4c), the bands at around 840 and 798 cm^{-1} can be assigned as the asymmetric and symmetric stretching mode of MoO_6. The wide band at 734 cm^{-1} is attributed to the asymmetric stretching mode of MoO_6. The bands at 578 cm^{-1} correspond to the bending vibration of MoO_6 [37]. Some absorption bands of Fe_3O_4/SiO_2 also still present in $Fe_3O_4/SiO_2/Bi_2MoO_6$ composite, obviously demonstrating that the Fe_3O_4/SiO_2 nanospheres are successful immobilized on the surface of flower-like Bi_2MoO_6 nanosheets.

Fig. 5 presents the magnetic hysteresis loops of the as-prepared Fe_3O_4, Fe_3O_4/SiO_2 and $Fe_3O_4/SiO_2/Bi_2MoO_6$ composite. All of these materials show superparamagnetic behavior owing to the ultrafine Fe_3O_4 nanocrystals at room temperature. The magnetic saturation (Ms) value of Fe_3O_4 nanoparticle is 78 emu g^{-1} [38], whereas those of Fe_3O_4/SiO_2 nanoparticles and $Fe_3O_4/SiO_2/Bi_2MoO_6$ composite are 36 and 5 emu g^{-1}, respectively. The magnetic separability of $Fe_3O_4/SiO_2/Bi_2MoO_6$ composite was examined in water by placing a magnet beside the glass bottle. Notably, the brown powder is easily attracted by the magnet, and thus can be conveniently collected. This will offer a simple and effortless way for efficiently separate magnetic photocatalyst from a suspension system by applying external magnetic field.

The UV–vis diffuse reflectance spectra (DRS) of the as-prepared samples are shown in Fig. 6. The spectrum of pure Bi_2MoO_6 microsphere exhibits the photosbsorption property from the UV light region to visible light until 490 nm, which can be assigned to a band gap of ~2.71 eV [39]. Apparently, $Fe_3O_4/SiO_2/Bi_2MoO_6$ composite shows more intensive absorption within the visible light range in comparison with pure Bi_2MoO_6 microspheres because of the incorporation of the black body properties of Fe_3O_4. Such enhancement of the absorption intensity, as well as superparamagnetism, implies that $Fe_3O_4/SiO_2/Bi_2MoO_6$ composite should be a good candidate for large-scale application of photocatalytic technique.

3.2. Photocatalytic study of $Fe_3O_4/SiO_2/Bi_2MoO_6$ composite

The photocatalytic activity of $Fe_3O_4/SiO_2/Bi_2MoO_6$ composite was evaluated by the degradation of RhB in aqueous solution under visible-light irradiation. Fig. 7a displays the time-dependent UV–vis absorption spectra of RhB solution in the presence of $Fe_3O_4/SiO_2/Bi_2MoO_6$ composite. It is found that the absorption of RhB in the visible light region rapidly decreases with the increase of irradiation time, and nearly disappears after 120 min, which implies the complete destruction of conjugated structure. In the meantime, there is a hypsochromic shift of absorption maximum from 554 nm to 500 nm corresponds to a step-by-step de-ethylation of RhB, accompanied with the color change from the initial pink to light yellow [39–41]. Fig. 7b represents the variation of RhB concentration (C/C_0) with irradiation time over different photocatalysts. The blank test without photocatalyst obviously suggests that the

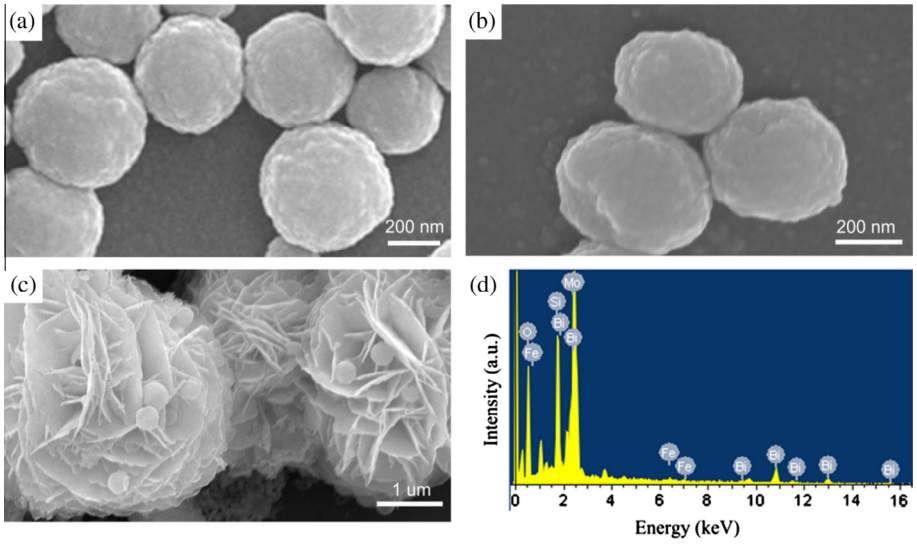

Fig. 2. SEM images of (a) Fe_3O_4, (b) Fe_3O_4/SiO_2, (c) $Fe_3O_4/SiO_2/Bi_2MoO_6$ composite and (d) EDX pattern of $Fe_3O_4/SiO_2/Bi_2MoO_6$ composite.

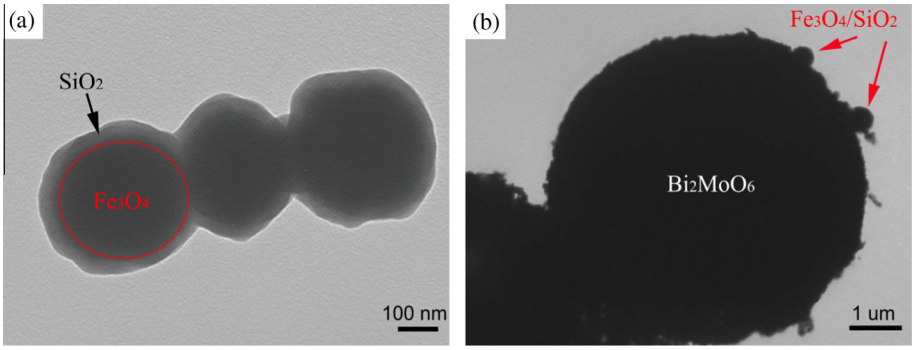

Fig. 3. TEM images of (a) Fe_3O_4/SiO_2 and (b) $Fe_3O_4/SiO_2/Bi_2MoO_6$ composite.

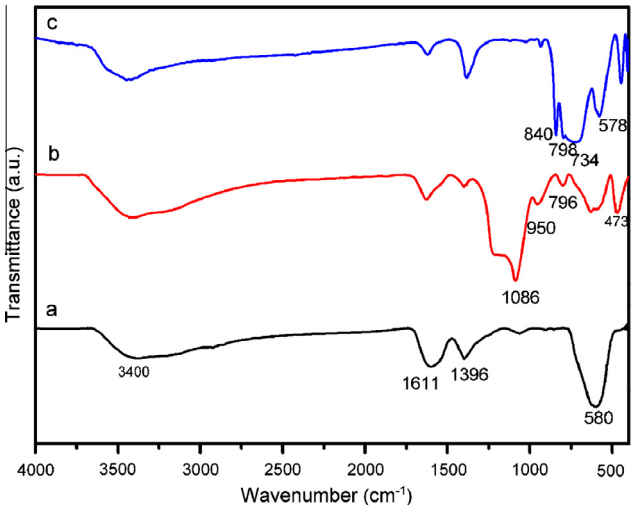

Fig. 4. FT-IR spectra of (a) Fe_3O_4, (b) Fe_3O_4/SiO_2 and (c) $Fe_3O_4/SiO_2/Bi_2MoO_6$ composite.

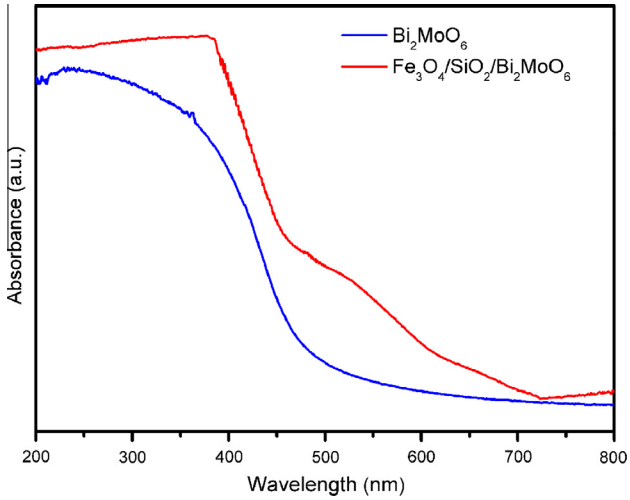

Fig. 6. UV–vis DRS of Pure Bi_2MoO_6 and $Fe_3O_4/SiO_2/Bi_2MoO_6$ composite.

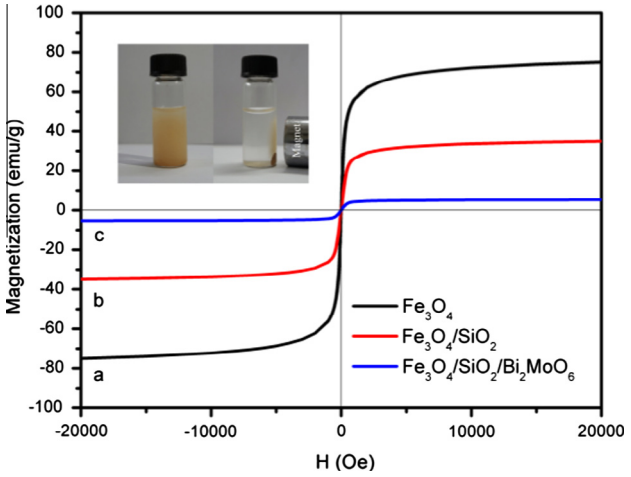

Fig. 5. Magnetization curves of the Fe_3O_4, Fe_3O_4/SiO_2 and $Fe_3O_4/SiO_2/Bi_2MoO_6$ composite. Insert pictures show the composite were easily dispersed in water (left) and easy separation by magnet (right).

self-photolysis process of RhB is extremely slow. Once pure Bi_2MoO_6 and $Fe_3O_4/SiO_2/Bi_2MoO_6$ composite are added, RhB is quickly decomposed, and the degradation efficiency reaches 96% and almost 100% respectively within 120 min. The improved photocatalytic activity of $Fe_3O_4/SiO_2/Bi_2MoO_6$ composite should be attributed to the make best use of the solar light compared with Bi_2MoO_6 microspheres (see Fig. 6). For comparison purposes, a commonly used photocatalyst, TiO_2 (Degussa P25) was also used as a reference for the degradation of RhB. The photocatalytic decomposition of RhB over P25 is 19% after an irradiation of 120 min, which can be ascribed to dye-sensitized effect.

In order to quantitatively understand the reaction kinetics of RhB, we also employed the pseudo-first-order model to fit the photocatalytic data. The model is expressed by $\ln(C_0/Ct) = kt$, where C_0 and C are the concentrations of pollutant in solution at time t_0 and t, respectively, and k is the apparent first-order rate constant [42,43]. As displayed in Fig. 7c, all the plots of $\ln(C_0/C)$ versus irradiation time (t) are nearly linear, indicating good linear dependence relations. The apparent rate constant k for the $Fe_3O_4/SiO_2/Bi_2MoO_6$ composite, Bi_2MoO_6 microspheres and P25 are calculated to be 0.02898, 0.02248 and 0.00176 min^{-1}, respectively. That is, the photocatalytic activity of $Fe_3O_4/SiO_2/Bi_2MoO_6$ composite is about 16.5-fold higher than that of P25, suggesting that $Fe_3O_4/SiO_2/Bi_2MoO_6$ composite should be an ideal photocatalytic material to replace TiO_2-based materials.

Considering that photodegradation may be caused by a dye-sensitized path when organic dyes such as RhB were selected as model pollutants, a colorless pollutant would be a better choice to demonstrate the photocatalytic activities of $Fe_3O_4/SiO_2/Bi_2MoO_6$ composite. Therefore, besides RhB, 2,4-dichlorophenol was also used as the another target so as to rule out the possibility of dye sensitization. As shown in Fig. S1, over 70% of 2,4-dichlorophenol molecules are decomposed after 5 h of visible light irradiation, further suggesting that $Fe_3O_4/SiO_2/Bi_2MoO_6$ composite possesses an excellent visible-light photocatalytic performance.

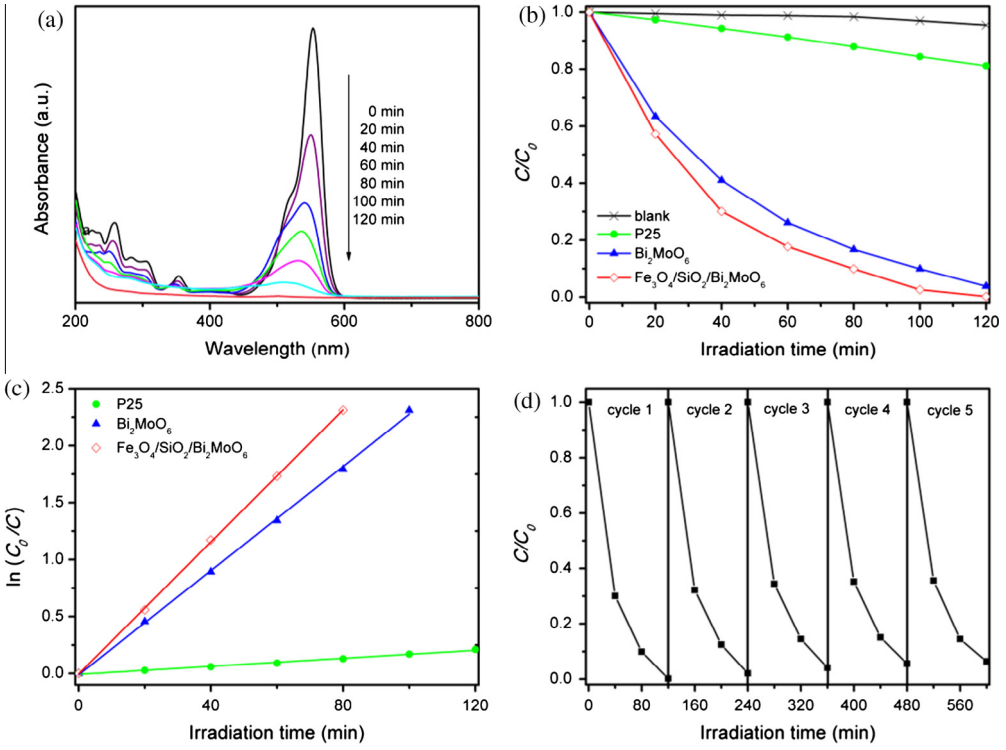

Fig. 7. (a) Absorption spectra of RhB with irradiation time over $Fe_3O_4/SiO_2/Bi_2MoO_6$. (b) Degradation rates of RhB under visible light irradiation without catalyst and in the presence of P25, Bi_2MoO_6, and $Fe_3O_4/SiO_2/Bi_2MoO_6$ composite. (c) First-order kinetics data for the photodegradation of RhB over P25, Bi_2MoO_6, and $Fe_3O_4/SiO_2/Bi_2MoO_6$ composite. (d) Cycling runs for the photocatalytic degradation of RhB in the presence of $Fe_3O_4/SiO_2/Bi_2MoO_6$ composite.

Furthermore, we also investigated the stability and reusability of $Fe_3O_4/SiO_2/Bi_2MoO_6$ composite. Given that superparamagnetism of composite, when each photocatalytic reaction is completed, photocatalyst can be easily separated under an external magnetic field for next reaction. Fig. 7d lists the results of five cyclic tests. After reusing 5 cycles, the degradation rate of RhB occurs a slight decrease, but it still remains ~90%. Therefore, $Fe_3O_4/SiO_2/Bi_2MoO_6$ composite would be a widely used photocatalyst in the future.

3.3. The role of silica layer of $Fe_3O_4/SiO_2/Bi_2MoO_6$ composite

It has been reported that the conduct band edge potential for Bi_2MoO_6, Fe_3O_4 and SiO_2 are −0.32, +1.23 and −4.10 eV, while the valence band edge potential for those are +2.39, +1.33 and +4.80 eV, respectively [27,44,45]. Apparently, only Bi_2MoO_6 can be activated by visible light irradiation to yield photogenerated electrons and holes. In consideration of more positive conduct band and more negative valence band of Fe_3O_4, both the photogenerated electrons and holes transfer from Bi_2MoO_6 to Fe_3O_4 before the introduction of SiO_2 (Fig. S2a). Such transfer will greatly accelerate the recombination of photogenerated electrons and holes originate from extremely narrow band gap (0.1 eV) of Fe_3O_4, which acts as a recombination center. As shown in Fig. S2b, once isolation layer of SiO_2 is introduced, transmission path of photogenerated carries between Bi_2MoO_6 and Fe_3O_4 is cut off, and thus avoids the loss of visible light photocatalytic activity of Bi_2MoO_6.

3.4. Possible photocatalytic mechanism of $Fe_3O_4/SiO_2/Bi_2MoO_6$ composite

Based on the above analysis, we also discussed possible photocatalytic mechanism of $Fe_3O_4/SiO_2/Bi_2MoO_6$ composite. Since the conduct band edge potential of Bi_2MoO_6 is more negative than the redox potential of $O_2/O_2^{\cdot-}$ (−0.28 eV) [46], the photogenerated electrons can reduce the adsorbed O_2 on the surface of Bi_2MoO_6 to form superoxide radical species $O_2^{\cdot-}$, which are a powerful oxidizing agent to degrade most dye molecules. The valence band edge potential of Bi_2MoO_6 is more positive than that of $^{\cdot}OH/OH^-$ (2.27 eV) [46], indicates that the photogenerated holes (h^+) are able to directly decompose dye molecules, as well as react with H_2O and produce hydroxyl radicals $^{\cdot}OH$ to decompose dye molecules. In other words, $O_2^{\cdot-}$, h^+ and $^{\cdot}OH$ could be the main active species for the photodegradation of RhB over $Fe_3O_4/SiO_2/Bi_2MoO_6$ composite. Thus, the trapping experiments were also used to further determine the main oxidant species. Benzoquinone (BQ, 0.1 mM), disodium ethylenediaminetetraacetate (EDTA, 2 mM), and tertbutyl alcohol (TBA, 2 mM) were used as a superoxide radicals scavenger, a hole scavenger and a hydroxyl radical scavenger, respectively (Fig. S3). Results distinctly indicate that the main oxidant species are $O_2^{\cdot-}$ and $^{\cdot}OH$ rather than h^+, which is in accordance with electron paramagnetic resonance (EPR) result reported in literature [47]. A hypothetical mechanism is proposed as follows:

$$Bi_2MoO_6 + h\nu(\text{visible light}) \rightarrow Bi_2MoO_6(e^- + h^+) \quad (1)$$

$$Bi_2MoO_6(e^-) + O_2 \rightarrow Bi_2MoO_6 + O_2^{\cdot-} \quad (2)$$

$$Bi_2MoO_6(h^+) + H_2O \rightarrow Bi_2MoO_6 + OH^{\cdot} + H^+ \quad (3)$$

$$O_2^{\cdot-}/OH^{\cdot} + \text{dye molecules} \rightarrow \text{degradation products} \quad (4)$$

4. Conclusions

In summary, we successfully developed a novel magnetically retrievable Bi_2MoO_6 photocatalyst through a simple hydrothermal method. The resulting $Fe_3O_4/SiO_2/Bi_2MoO_6$ composite possess a hierarchical structure consisting of flower-like three dimensional (3D) Bi_2MoO_6 microspheres and Fe_3O_4/SiO_2 magnetic nanoparticles. In view of the integration of Fe_3O_4/SiO_2 magnetic

nanoparticles, the samples can be easily separated and collected from the dispersed suspension by applying an external magnetic field. The visible light photocatalytic tests show that the present $Fe_3O_4/SiO_2/Bi_2MoO_6$ composite own an excellent photocatalytic activity for degrading RhB higher than that of individual Bi_2MoO_6, as well as the nanosized TiO_2. Such a composite photocatalyst is a promising photocatalytic material for removing harmful organic dyes in waste water. However, the surface area of present $Fe_3O_4/SiO_2/Bi_2MoO_6$ composite is quite low ($S_{BET} < 10\ m^2\ g^{-1}$). Therefore, our future work would focus on constructing structures with large surface areas to further improve the photocatalytic activity.

Acknowledgements

We thank National Natural Science Foundation of China (Nos. 51010005, 91216123 and 51174063), Natural Science Funds for Distinguished Young Scholar of Heilongjiang Province, The Natural Science Foundation of Heilongjiang Province (E201436), The International Science & Technology Cooperation Program of China (2013DFR10630) and Specialized Research Fund for the Doctoral Program of Higher Education (SRFDP 20132302110031).

Appendix A. Supplementary material

Supplementary data associated with this article can be found, in the online version, at http://dx.doi.org/10.1016/j.jallcom.2015.03.039.

References

[1] M.R. Hoffmann, S.T. Martin, W.Y. Choi, D.W. Bahnemann, Environmental applications of semiconductor photocatalysis, Chem. Rev. 95 (1995) 69–96.
[2] R. Asahi, T. Morikawa, T. Ohwaki, K. Aoki, Y. Taga, Visible-light photocatalysis in nitrogen-doped titanium oxides, Science 293 (2001) 269–271.
[3] H. Tong, S.X. Ouyang, Y.P. Bi, N. Umezawa, M. Oshikiri, J.H. Ye, Nano-photocatalytic materials: possibilities and challenges, Adv. Mater. 24 (2012) 229–251.
[4] W.Y. Teoh, J.A. Scott, R. Amal, Progress in heterogeneous photocatalysis: from classical radical chemistry to engineering nanomaterials and solar reactors, J. Phys. Chem. Lett. 3 (2012) 629–639.
[5] Y. Park, S.H. Lee, S.O. Kang, W. Choi, Organic dye-sensitized TiO_2 for the redox conversion of water pollutants under visible light, Chem. Commun. 46 (2010) 2477–2479.
[6] Y.L. Tian, J. Fu, B.B. Chang, F.N. Xi, X.P. Dong, Synthesis of mesoporous CdS/titania composites with visible light photocatalytic activities, Mater. Lett. 81 (2012) 95–98.
[7] A. Kudo, Y. Miseki, Heterogeneous photocatalyst materials for water splitting, Chem. Soc. Rev. 38 (2009) 253–278.
[8] Z. Luo, L. Qu, T. Han, Z. Zhang, X. Shao, X. Wu, Z.-L. Chen, Magnetite/Bi-doped carboxylate-rich carbon spheres-a highly efficient magnetic photocatalyst based on dimetallic Fe-II/Fe-III and Bi-III/Bi-IV photoredox cycles, Eur. J. Inorg. Chem. 2014 (2014) 994–1000.
[9] S. Ye, L.G. Qiu, Y.P. Yuan, Y.J. Zhu, J. Xia, J.F. Zhu, Facile fabrication of magnetically separable graphitic carbon nitride photocatalysts with enhanced photocatalytic activity under visible light, J. Mater. Chem. A 1 (2013) 3008–3015.
[10] S.W. Zhang, J.X. Li, M.Y. Zeng, G.X. Zhao, J.Z. Xu, W.P. Hu, X.K. Wang, In situ synthesis of water-soluble magnetic graphitic carbon nitride photocatalyst and its synergistic catalytic performance, ACS Appl. Mater. Interfaces 5 (2013) 12735–12743.
[11] S.H. Xuan, W.Q. Jiang, X.L. Gong, Y. Hu, Z.Y. Chen, Magnetically separable Fe_3O_4/TiO_2 hollow spheres: fabrication and photocatalytic activity, J. Phys. Chem. C 113 (2009) 553–558.
[12] C.W. Tan, G.Q. Zhu, M. Hojamberdiev, C. Xu, J. Liang, P.F. Luo, Y. Liu, Room temperature synthesis and photocatalytic activity of magnetically recoverable Fe_3O_4/BiOCl nanocomposite photocatalysts, J. Clust. Sci. 24 (2013) 1115–1126.
[13] G.P. Li, L.Q. Mao, Magnetically separable Fe_3O_4–Ag_3PO_4 sub-micrometre composite: facile synthesis, high visible light-driven photocatalytic efficiency, and good recyclability, Rsc Adv. 2 (2012) 5108–5111.
[14] M.M. Ye, Q. Zhang, Y.X. Hu, J.P. Ge, Z.D. Lu, L. He, Z.L. Chen, Y.D. Yin, Magnetically recoverable core–shell nanocomposites with enhanced photocatalytic activity, Chem-Eur. J. 16 (2010) 6243–6250.
[15] Y. Wang, S.K. Li, X.R. Xing, F.Z. Huang, Y.H. Shen, A.J. Xie, X.F. Wang, J. Zhang, Self-assembled 3D flowerlike hierarchical $Fe_3O_4@Bi_2O_3$ core–shell architectures and their enhanced photocatalytic activity under visible light, Chem-Eur. J. 17 (2011) 4802–4808.
[16] L. Zhang, W.Z. Wang, M. Shang, S.M. Sun, J.H. Xu, Bi_2WO_6@carbon/Fe_3O_4 microspheres: preparation, growth mechanism and application in water treatment, J. Hazard. Mater. 172 (2009) 1193–1197.
[17] X.W. Li, C.G. Niu, D.W. Huang, X.Y. Wang, X.G. Zhang, G.M. Zeng, Q.Y. Niu, Preparation of magnetically separable Fe_3O_4/BiOI nanocomposites and its visible photocatalytic activity, Appl. Surf. Sci. 286 (2013) 40–46.
[18] Z. Liu, F.T. Chen, Y.P. Gao, Y. Liu, P.F. Fang, S.J. Wang, A novel synthetic route for magnetically retrievable Bi_2WO_6 hierarchical microspheres with enhanced visible photocatalytic performance, J. Mater. Chem. A 1 (2013) 7027–7030.
[19] G.H. Tian, Y.J. Chen, W. Zhou, K. Pan, Y.Z. Dong, C.G. Tian, H.G. Fu, Facile solvothermal synthesis of hierarchical flower-like Bi_2MoO_6 hollow spheres as high performance visible-light driven photocatalysts, J. Mater. Chem. 21 (2011) 887–892.
[20] Z.Q. Li, X.T. Chen, Z.L. Xue, Bi_2MoO_6 microstructures: controllable synthesis, growth mechanism, and visible-light-driven photocatalytic activities, CrystEngComm 15 (2013) 498–508.
[21] G.H. Tian, Y.J. Chen, R.T. Zhai, J. Zhou, W. Zhou, R.H. Wang, K. Pan, C.G. Tian, H.G. Fu, Hierarchical flake-like Bi_2MoO_6/TiO_2 bilayer films for visible-light-induced self-cleaning applications, J. Mater. Chem. A 1 (2013) 6961–6968.
[22] Y. Shimodaira, H. Kato, H. Kobayashi, A. Kudo, Photophysical properties and photocatalytic activities of bismuth molybdates under visible light irradiation, J. Phys. Chem. B 110 (2006) 17790–17797.
[23] M.T. Montero, P. Millan, P. Duran-Martin, B. Jimenez, A. Castro, Solid solutions of lead-doped bismuth layer of Aurivillius $n = 2$ and $n = 3$ oxides: structural and dielectric characterization, Mater. Res. Bull. 33 (1998) 1103–1115.
[24] B. Frit, J.P. Mercurio, The crystal-chemistry and dielectric-properties of the Aurivillius family of complex bismuth oxides with perovskite-like layered structures, J. Alloys Comp. 188 (1992) 27–35.
[25] L. Zhou, W.Z. Wang, L.S. Zhang, Ultrasonic-assisted synthesis of visible-light-induced Bi_2MO_6 (M = W, Mo) photocatalysts, J. Mol. Catal. A-Chem. 268 (2007) 195–200.
[26] W.Z. Yin, W.Z. Wang, S.M. Sun, Photocatalytic degradation of phenol over cage-like Bi_2MoO_6 hollow spheres under visible-light irradiation, Catal. Commun. 11 (2010) 647–650.
[27] M.C. Long, W.M. Cai, H. Kisch, Visible light induced photoelectrochemical properties of n-$BiVO_4$ and n-$BiVO_4$/p-CO_3O_4, J. Phys. Chem. C 112 (2008) 548–554.
[28] L.W. Zhang, T.G. Xu, X. Zhao, Y.F. Zhu, Controllable synthesis of Bi_2MoO_6 and effect of morphology and variation in local structure on photocatalytic activities, Appl. Catal. B-Environ. 98 (2010) 138–146.
[29] J.H. Bi, L. Wu, H. Li, Z.H. Li, X.X. Wang, X.Z. Fu, Simple solvothermal routes to synthesize nanocrystalline Bi_2MoO_6 photocatalysts with different morphologies, Acta Mater. 55 (2007) 4699–4705.
[30] M.Y. Zhang, C.L. Shao, J.B. Mu, Z.Y. Zhang, Z.C. Guo, P. Zhang, Y.C. Liu, One-dimensional Bi_2MoO_6/TiO_2 hierarchical heterostructures with enhanced photocatalytic activity, CrystEngComm 14 (2012) 605–612.
[31] P. Zhang, C.L. Shao, M.Y. Zhang, Z.C. Guo, J.B. Mu, Z.Y. Zhang, X. Zhang, Y.C. Liu, Bi_2MoO_6 ultrathin nanosheets on $ZnTiO_3$ nanofibers: a 3D open hierarchical heterostructures synergistic system with enhanced visible-light-driven photocatalytic activity, J. Hazard. Mater. 217 (2012) 422–428.
[32] J. Liu, Z.K. Sun, Y.H. Deng, Y. Zou, C.Y. Li, X.H. Guo, L.Q. Xiong, Y. Gao, F.Y. Li, D.Y. Zhao, Highly water-dispersible biocompatible magnetite particles with low cytotoxicity stabilized by citrate groups, Angew. Chem. Int. Edit. 48 (2009) 5875–5879.
[33] Y. Deng, D. Qi, C. Deng, X. Zhang, D. Zhao, Superparamagnetic high-magnetization microspheres with an $Fe_3O_4@SiO_2$ core and perpendicularly aligned mesoporous SiO_2 shell for removal of microcystins, J. Am. Chem. Soc. 130 (2008) 28–29.
[34] H.F. Men, H.Q. Liu, Z.L. Zhang, J. Huang, J. Zhang, Y.Y. Zhai, L. Li, Synthesis, properties and application research of atrazine $Fe_3O_4@SiO_2$ magnetic molecularly imprinted polymer, Environ. Sci. Pollut. R 19 (2012) 2271–2280.
[35] Y. Chi, Q. Yuan, Y.J. Li, J.C. Tu, L. Zhao, N. Li, X.T. Li, Synthesis of $Fe_3O_4@SiO_2$–Ag magnetic nanocomposite based on small-sized and highly dispersed silver nanoparticles for catalytic reduction of 4-nitrophenol, J. Colloid Interf. Sci. 383 (2012) 96–102.
[36] J.H. Bi, J.G. Che, L. Wu, M.H. Liu, Effects of the solvent on the structure, morphology and photocatalytic properties of Bi_2MoO_6 in the solvothermal process, Mater. Res. Bull. 48 (2013) 2071–2075.
[37] H.H. Li, K.W. Li, H. Wang, Hydrothermal synthesis and photocatalytic properties of bismuth molybdate materials, Mater. Chem. Phys. 116 (2009) 134–142.
[38] M.F. Shao, F.Y. Ning, J.W. Zhao, M. Wei, D.G. Evans, X. Duan, Preparation of $Fe_3O_4@SiO_2$@ layered double hydroxide core–shell microspheres for magnetic separation of proteins, J. Am. Chem. Soc. 134 (2012) 1071–1077.
[39] F. Chen, J.C. Zhao, H. Hidaka, Highly selective deethylation of Rhodamine B: adsorption and photooxidation pathways of the dye on the TiO_2/SiO_2 composite photocatalyst, Int. J. Photoenergy 5 (2003) 209–217.
[40] X. Xu, X.P. Shen, G.X. Zhu, L.Q. Jing, X.S. Liu, K.M. Chen, Magnetically recoverable Bi_2WO_6–Fe_3O_4 composite photocatalysts: fabrication and photocatalytic activity, Chem. Eng. J. 200 (2012) 521–531.

[41] A. Phuruangrat, P. Jitrou, P. Dumrongrojthanath, N. Ekthammathat, B. Kuntalue, S. Thongtem, T. Thongtem, Hydrothermal synthesis and characterization of Bi_2MoO_6 nanoplates and their photocatalytic activities, J. Nanomater. 2013 (2013) 1–8.
[42] L. Li, Y.L. Yang, X.R. Liu, R.Q. Fan, Y. Shi, S. Li, L.Y. Zhang, X. Fan, P.X. Tang, R. Xu, W.Z. Zhang, Y.Z. Wang, L.Q. Ma, A direct synthesis of B-doped TiO_2 and its photocatalytic performance on degradation of RhB, Appl. Surf. Sci. 265 (2013) 36–40.
[43] X. Xiao, R. Hao, X.X. Zuo, J.M. Nan, L.S. Li, W.D. Zhang, Microwave-assisted synthesis of hierarchical $Bi_7O_9I_3$ microsheets for efficient photocatalytic degradation of bisphenol-A under visible light irradiation, Chem. Eng. J. 209 (2012) 293–300.
[44] Y. Xu, M.A.A. Schoonen, The absolute energy positions of conduction and valence bands of selected semiconducting minerals, Am. Mineral. 85 (2000) 543–556.
[45] X. Lin, X.Y. Guo, D. Liu, Q.W. Wang, H.J. Zhai, L.M. Chang, SiO_2/Bi_2MoO_6 nanocomposites with high photocatalytic activity under visible light irradiation, Mater. Res. Bull. 63 (2015) 72–79.
[46] A. Fujishima, T.N. Rao, D.A. Tryk, Titanium dioxide photocatalysis, J. Photochem. Photobiol. 1 (2000) 1–21.
[47] J.L. Long, S.C. Wang, H.J. Chang, B.Z. Zhao, B.T. Liu, Y.G. Zhou, W. Wei, X.X. Wang, L. Huang, W. Huang, Bi_2MoO_6 nanobelts for crystal facet-enhanced photocatalysis, Small 10 (2014) 2791–2795.